Побудована фізична модель імпульсного торцевого ущільнення як системи автоматичного регулювання торцового зазору і протікання.

Вивчено вплив параметрів імпульсного ущільнення на його статичні характеристики. Проведений аналіз статичних характеристик дозволив виявити вплив конструктивних параметрів імпульсного ущільнення на величину торцового зазору і витоків ущільнюваної рідини. Зроблено висновки про вплив коефіцієнта навантаження і зусилля попереднього стиснення пружин на статичні характеристики імпульсного ущільнення. Статичний розрахунок дозволяє визначити коефіцієнт гідростатичної жорсткості, умови статичної стійкості, діапазон допустимих ущільнюваних тисків.

Визначено фактори, що впливають на динамічні характеристики ущільнення. Проведено оцінку розмірних значень амплітуд вимушених осьових коливань кільця на будь-якій частоті обертання. Отримані вирази амплітудних і фазових частотних характеристик, що дозволяють виявити небезпечні області частот обертання і підібрати параметри ущільнення так, щоб амплітуди вимушених осьових коливань кільця не виходили за межі динамічної стійкості. Виявлено, що область стійкості розширюється за рахунок зменшення обсягу камер і зменшення коефіцієнта гидростатичної жорсткості.

Запропоновано методику аналітичного розрахунку імпульсних торцових ущільнень, що дозволяє розраховувати геометрію ущільнення на етапі його проектування. Наведено приклад інженерного розрахунку імпульсного торцового ущільнення, а також конструкцію вузла ущільнення, спроектованого за запропонованою методикою

Ключові слова: імпульсне торцове ущільнення, статичні характеристики, амплітудні і фазові характеристики, динамічна стійкість

UDC 621.01:62-251:62-762
DOI: 10.15587/1729-4061.2020.206721

DEVELOPMENT OF METHODS TO CALCULATE A PULSE MECHANICAL SEAL ON THE BASIS OF ITS PHYSICAL MODEL CONSTRUCTION

S. Shevchenko
PhD, Technical Director
LLC United Production - Atom
Prokofiev str., 36, Sumy, Ukraine, 40014
E-mail: s.shevchenko@united.productions
A. Chernov
PhD, Director
LLC "Design Bureau "UkrSpetsMash"
Promyslova str., 6, Sumy, Ukraine, 40018
E-mail: alexch07@ukr.net

Received date 13.05.2020
Accepted date 15.06.2020
Published date 30.06.2020

1. Introduction

A pulse mechanical seal belongs to non-contact seals with self-adjusting clearance; as an alternative to hydrostatic and hydrodynamic non-contact mechanical seals, it was invented during the creation of rotor seals of the main circulation pumps for nuclear power plants [1]. Comprehensive experimental studies and full-scale tests have shown that pulse seals meet the stringent requirements for reliability, tightness and resource life required for the main equipment of nuclear power plants [2]. Due to their high performance characteristics, pulse mechanical seals have attracted the attention of developers of high-speed centrifugal machines for other industries, in particular, for fuel pumps of liquid-propellant rocket engines (LPREs) [3, 4]. Pulse seals were also the prototype of promising gate mechanical seals with a coaxial arrangement of steps.

Pulse mechanical seals with self-adjusting clearance have a number of undeniable advantages compared to conventional mechanical seals and non-contact mechanical seals of hydrostatic and hydrodynamic types. In conventional mechanical seals, the friction power is proportional to the sealing pressure and the peripheral speed; therefore, their operability is preserved only in a narrow, calculated range of operating parameters—the sealing pressure and the rotation speed. In pulse seals, an increase in the rotation frequency results in a larger end clearance, and the friction power losses practically do not increase, thus making their use especially effective for high-speed machines. Low losses of friction power and good heat dissipation with leakage from the friction pair make it sometimes possible to do without additional cooling systems even in pumps running on hot liquids, for example, in feed pumps of nuclear and thermal power plants.

By proper selection of the basic geometric parameters of the friction pair of a pulse seal, it is possible to ensure the optimal value of the end clearance, the required leakage and power loss in the friction pair in a wide range of sealing pressures and rotor speeds. Therefore, the development of methods for calculating pulse mechanical seals based on a study of their working processes is relevant.

2. Literature review and problem statement

Analysis of previous publications shows that a number of studies describe the design of non-contact mechanical

fluid and gas seals [5, 6], the principle of work [7], as well as methods of calculation and experimental tests of non-contact mechanical seals with dynamic grooves for pumps and compressors [8]. The contactless operation of such seals is ensured by the implementation of micro-grooves of various shapes on one of the sealing surfaces the depth of which is commensurate with the size of the end clearance. The manufacture of such seals requires the use of expensive precision methods for machining friction pair rings. In addition, existing methods for calculating them, as a rule, are based on a numerical solution of the equations of flow of a liquid or gas and there are no simple analytical dependencies for calculating static and dynamic characteristics that help evaluate the geometry of the sealing assembly at the design stage. Methods for calculating mechanical seals using modern computer programs based on numerical finite element methods are described in [9, 10].

In conventional mechanical seals, the friction power is proportional to the sealing pressure and the peripheral speed; therefore, their operability is preserved only in a narrow, calculated range of operating parameters—the sealing pressure and the rotation speed [11]. In the designs of hydrostatic and hydrodynamic non-contact mechanical seals, the pressure force of the locking medium is perceived by an axially movable ring. With increasing pressure of the locking medium, the gap becomes larger [12, 13].

Pulse mechanical seals are devoid of the listed disadvantages [14, 15]. For their successful design, a methodology for calculating the basic geometric dimensions of a seal is needed to ensure the required tightness under given operating conditions. To obtain analytical calculated dependencies, it is necessary to build a physical model of a pulse mechanical seal and to study its static and dynamic characteristics.

3. The aim and objectives of the study

The aim of the study is to build a physical model of a mechanical sealing mechanism that will help obtain analytical dependencies for its calculation at the design stage.

To achieve the aim, the following tasks were set and done:

– to obtain analytical dependencies for constructing the static characteristics of mechanical pulse compaction and evaluate the influence of structural parameters on them. Determine the coefficient of hydrostatic stiffness, the condition of static stability, and the range of permissible sealing pressures;

– to analyze the amplitude and phase frequency characteristics of the pulse mechanical seal.

4. Building a physical model of pulse mechanical compaction

The simplest design of a single-stage pulse compaction unit is shown in Fig. 1. A pulse seal differs from a mechanical seal in the following design features. Closed chambers 2 are located on the end surface of the axial-movable ring 1, and several radial feed channels 5 are made on the rotating support ring 6 and are open towards the cavity to be sealed. Through these channels, the medium to be sealed is injected into the chambers under a sealing pressure p_1 for those short periods of time $t_c = \beta_c / \omega$ during which the rotating channels 5 pass by the chambers 2. At these moments, the pressure p_2 in the chambers increases abruptly to $p_{2\max}=p_1$ minus the inertial pressure $p_* = 0.5\rho\left(r_3^2 - r_2^2\right)\omega^2$ that occurs in the rotating radial feeding channels. By changing the shape of the feeders, it is possible to slightly change the value of p and thereby the value of $p_{2\max} = p_1 - p_*$. The inertial pressure can be eliminated completely by placing the feeders on a non-rotating ring and the chambers on a rotating ring. The influence of the inertial pressure on the characteristics of the seal will be ignored.

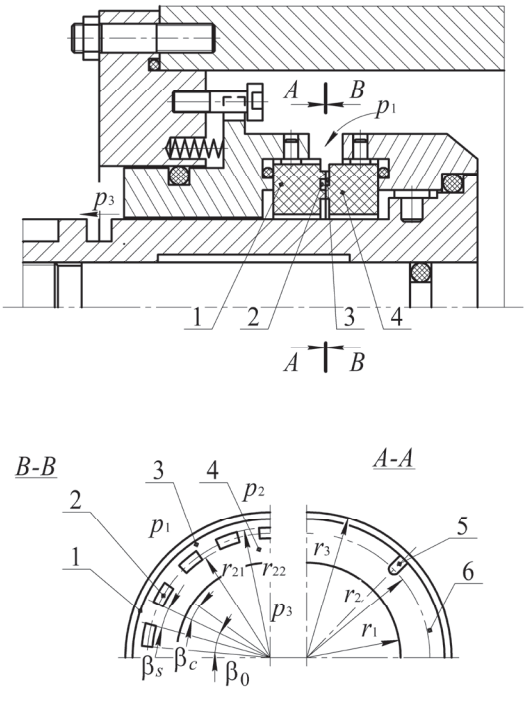

Fig. 1. The diagram of a pulse mechanical seal

Let us consider the nature of the change in pressure in the chamber over a period of $T = 2\pi / \omega n_i$ (n_i is the number of feeders) between two subsequent injections. The change in pressure depends on the hydraulic resistance g_i of the feeders and the conductivities of the internal (from the side of the pressurized pressure) 3 and the external 4 end clearance throttles $g_1(z)$ and $g_3(z)$.

Fig. 2 [15] shows approximate graphs of pressure changes in a separate chamber. The larger the gap, the smaller the $p_{2\min}$.

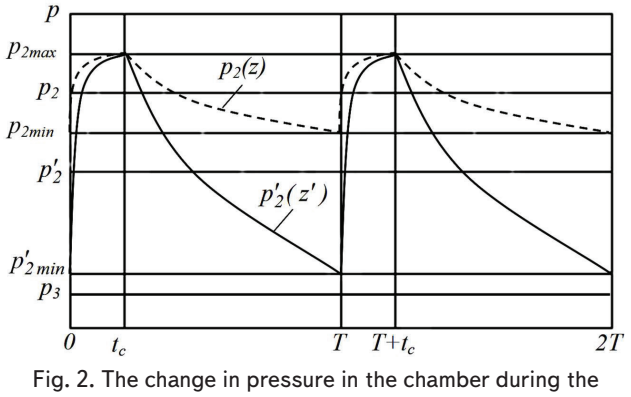

Fig. 2. The change in pressure in the chamber during the period T between injections

A similar picture takes place during the expansion process, when the feeder is located outside the sector β_c at

the time interval $T-t_c$. After the feeder leaves the sector β_c occupied by the chamber, the pressure p_2 in the chamber begins to decrease due to leakage of the compressed medium through the external flat gap 4; A_1 and A_3 are the wall areas of the flat annular gaps (Fig. 3). The pressure drop continues until the next injection (Fig. 2), and the drop depth, i. e., the value of $p_{2\min}$, depends on the size of the end clearance: the larger the gap, the smaller the $p_{2\min}$. Another possible combination of parameters is when the pressure reaches the minimum of p_3 in time of $t<T$. With a decrease in the gap, the amplitude of the pressure change in the chamber decreases, and the average pressure increases.

Thus, there is a negative feedback between the end clearance z (adjustable value) and the force F_s (regulatory effect), which ensures self-regulation of the end clearance (Fig. 5).

The operation of the seal is based on the creation of high-frequency pressure pulses in the discharge chambers; therefore, it is called a pulse seal.

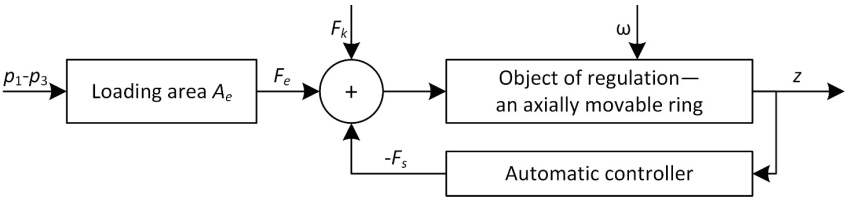

Fig. 5. The block diagram of pulse compaction as the automatic control system

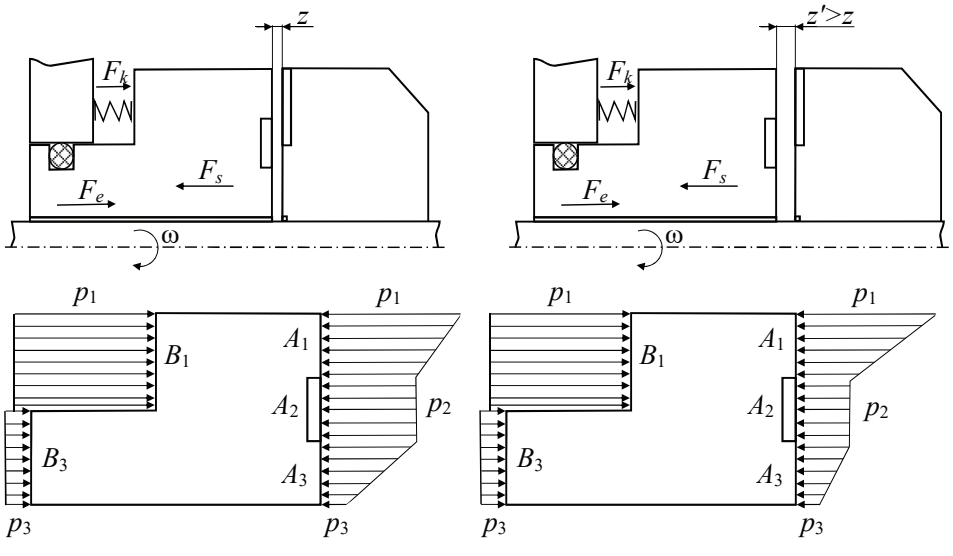

Fig. 3. The change in pressure on the end surfaces of the axially movable ring, depending on the end clearance: $z`>z$

The shorter the time between injections, the smaller the depth of the pressure drop $p_{2\min}$ in the chambers (Fig. 4), the greater the averaged pressure p_2 in the chambers and the greater the force F_s that opens the butt joint.

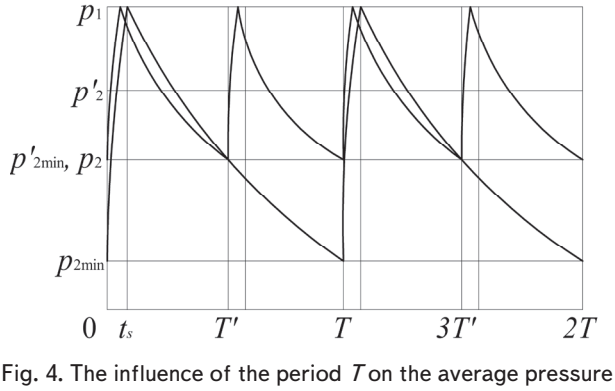

Fig. 4. The influence of the period T on the average pressure in the chambers: $T'=0.5T$

The pressure force $F_s(z)$ revealing the end joint, depends on the pressure $\overline{p}_2(z)$ and, accordingly, on the gap. As the gap decreases, it increases, and its balance with the external force F_e independent of the gap is violated. Under the action of an axially movable ring of the positive difference $F_s-F_e>0$, the gap decreases (Δz) so that the equality $F_s=F_e$ is restored.

5. Research on the influence of pulse compaction parameters on static characteristics

To estimate the pressure in the chambers, we will consider the radial flow of a viscous compressible fluid in a flat channel having the form of a sector with a central angle β_c and a radial size of r_3-r_1 formed by elements of the sealing surfaces and separated by a flow chamber (Fig. 1). The right wall of the gap on which the feeders are located rotates; the left wall has freedom of axial movement within the micron-size mechanical gap. The circumferential component of the flow is not taken into account.

The flow in the channels is unsteady. The feeder, passing over time $t_c=\beta_c/\omega$ through the chamber filled with liquid, spasmodically brings pressure p_1 to it. As a result, the pressure rises to the maximum value of p_1, compressing the liquid in the chamber. After the feeder leaves the sector β_c, the volume of the liquid compressed in the chamber flows out, and the pressure decreases to the initial minimum value. The expansion process takes place during the time $T-t_c$. After this, compression begins again, and the process repeats (Fig. 2).

During compression, the difference in the volumes of the liquid flowing in through the feeder and the internal end throttle $(Q_i+Q_1)\mathrm{d}t$ and flowing out $(Q_3\mathrm{d}t)$ through the outer throttle is compensated by the volume filling the volume $-\mathrm{d}V$ freed up as a result of the compression of the liquid in the chamber:

$$(Q_i+Q_1)\mathrm{d}t-Q_3\mathrm{d}t=-\mathrm{d}V. \quad (1)$$

In the process of expansion, the volume of the outflowing fluid $(Q_3\mathrm{d}t)$ is greater than the volume of the inflowing fluid $(Q_1\mathrm{d}t)$ by the amount of $\mathrm{d}V$ with the opposite sign:

$$Q_3\mathrm{d}t-Q_1\mathrm{d}t=\mathrm{d}V. \quad (2)$$

Equation (1) differs from (2) only in the flow rate through the feeder and in the initial condition: the compres-

sion starts from the minimum pressure, and the expansion starts from the maximum.

The bulk modulus of the fluid is

$$E = -V_0 \frac{\mathrm{d}p}{\mathrm{d}V},$$

whence

$$\mathrm{d}V = -\frac{V_0}{E}\mathrm{d}p,$$

where $\mathrm{d}V = V - V_0$ is the difference between the final V and initial V_0 volumes of the fluid, V_0 is the unchanged volume of the chamber, E is the isothermal volumetric modulus of elasticity of the fluid, Q_i is the flow rate through the feeder, and Q_1 and Q_3 are the flow rates through the internal and external end throttles of the sector β_c.

For a laminar flow, the costs linearly depend on the pressure drops:

$$Q_i = g_i(p_1 - p),\ \ Q_1 = g_1(p_1 - p),\ \ Q_3 = g_3(p - p_3). \qquad (3)$$

The conductivities of the mechanical throttles for laminar flows are proportional to the cube of the gap z [15] and are expressed by the formulae

$$g_1 = g_{1n}u^3,\ \ g_3 = g_{3n}u^3,\ \ u = z/z_n,$$

$$g_{1n} = \frac{\beta_c z_n^3}{12\mu \ln(r_3/r_{22})} \approx \frac{\beta_c z_n^3 r_3}{12\mu l_1},\ \ l_1 = r_3 - r_{22},$$

$$g_{3n} = \frac{\beta_c z_n^3}{12\mu \ln(r_{21}/r_1)} \approx \frac{\beta z^3 r_{21}}{12\mu l_3},\ \ l_3 = r_{21} - r_1,$$

z_n=(2...6) μm is the nominal end clearance adopted for this design, $u = z/z_n$ is the dimensionless current gap, and μ is the dynamic viscosity of the fluid being compacted.

Substituting the expressions of expenditures in (1) and (2) and dividing both sides of the equalities by dt, we obtain the equations of balance of volume expenditures. On the time intervals of compression $(0 \le t \le t_c)$ and expansion $(t_c \le t_* \le T - t_c)$ relative to the current pressure p_c, p_p in the chamber, we obtain inhomogeneous first-order differential equations:

$$\frac{V_0}{E}\frac{\mathrm{d}p_c}{\mathrm{d}t} = g_i(p_1 - p_c) + g_1(p_1 - p_c) - g_3(p_c - p_3),$$

$$\frac{V_0}{E}\frac{\mathrm{d}p_p}{\mathrm{d}t_*} = g_1(p_1 - p_p) - g_3(p_p - p_3),\ \ (t_* = t - t_c). \qquad (4)$$

After some transformations, the equations of pressure growth during compression and pressure drop during expansion in the chamber take the following form:

$$T_c\frac{\mathrm{d}p_c}{\mathrm{d}t} + p_c = \frac{1}{G}\left[\left(1 + \alpha_{1i}u^3\right)p_1 + \alpha_{3i}u^3 p_3\right] = G_c,$$

$$T_p\frac{\mathrm{d}p_p}{\mathrm{d}t_*} + p_p = \alpha_{e3}p_1 + \alpha_{e1}p_3 = G_p, \qquad (5)$$

where the constants of the time of filling and emptying the chamber, weight coefficients, dimensionless pressure and conductivity are expressed by the formulae:

$$T_c = \frac{\overline{T}_c}{G(u)},\ \ \overline{T}_c = \frac{V_0}{Eg_i},\ \ G(u) = 1 + (\alpha_{1i} + \alpha_{3i})u^3;$$

$$T_p = \frac{\overline{T}_p}{u^3},\ \ \overline{T}_p = \frac{V_0\alpha_{e3}}{Eg_{1n}},$$

$$G_c = \frac{1}{G}\left[\left(1 + \alpha_{1i}u^3\right)p_1 + \alpha_{3i}u^3 p_3\right],\ G_p = \alpha_{e3}p_1 + \alpha_{e1}p_3,$$

$$\alpha_{e3} = \frac{g_{en}}{g_{3n}},\ \ \alpha_{e1} = \frac{g_{en}}{g_{1n}} = 1 - \alpha_{e3},$$

$$\alpha_{1i} = \frac{g_{1n}}{g_i},\ \ \alpha_{3i} = \frac{g_{3n}}{g_i},\ \ \alpha_{31} = \frac{g_{3n}}{g_{1n}};$$

$$g_{en} = \frac{g_{1n}g_{3n}}{g_{1n} + g_{3n}},\ \ g_e = g_{en}u^3.$$

The sealing pressure p_1 and the back pressure p_3 are constant in time; therefore, introducing substitutions

$$p_c = p_c' + G_c,\ \ p_p = p_p' + G_p, \qquad (6)$$

we arrive at the homogeneous equations

$$T_c\frac{\mathrm{d}p_c'}{\mathrm{d}t} + p_c' = 0,\ T_p\frac{\mathrm{d}p_p'}{\mathrm{d}t} + p' = 0. \qquad (7)$$

The initial conditions necessary for solving equations (5) are determined based on the approximate graphs of the pressure change in the chamber during the periods of compression and expansion (Fig. 2). The end of compression means that $p_c \approx G_c$, and at the end of expansion means that $p_p \approx G_p$. Using these limit values, we obtain

$$p_c(0) \approx G_p,\ \ p_p(0) = p_c(t_c) \approx G_c.$$

To find a solution to the equations of (7), we will use the operational method. Let us denote the Laplace image of the desired pressure as $p_c'(t) \doteq P_c'(s)$, and the image of the derivative will be $\frac{\mathrm{d}p_c'}{\mathrm{d}t} \doteq sP_c' - p_c'(0)$. Substituting these expressions in the first equation of (7), we arrive at an algebraic equation for the image

$$(T_c s + 1)P_c'(s) - T_c p_c'(0) = 0,$$

where the pressure image is

$$P_c'(s) = \frac{T_c p_c'(0)}{T_c s + 1}.$$

Using the tables of inverse Laplace transforms, we obtain the original pressure as

$$p_c' = p_c'(0)e^{-\frac{t}{T_c}}. \qquad (8)$$

Taking into account (6) and the initial conditions, we finally have

$$p_c = G_A - (G_c - G_p)e^{-\frac{t}{T_c}}. \qquad (9)$$

In Fig. 6, the transient response of the compression is represented by the exponent in the time interval of $t \le t_c$. The characteristic asymptotically approaches the horizontal line of G_c=const, and the time constant T_c is numeri-

cally equal to the length of the tangent at the asymptote G_c=const. If we do not take into account the compressibility of the medium being compressed $(E\to\infty)$, then T_c=0, p_c=G_c, the pressure remains constant, and its value is determined by the ratio of the conductivities of the end throttles g_1, g_3 and feeders g_i. With unlimited growth of g_i, $\alpha_{1i}\approx\alpha_{3i}\approx 0$, and $p_c\approx p_1$.

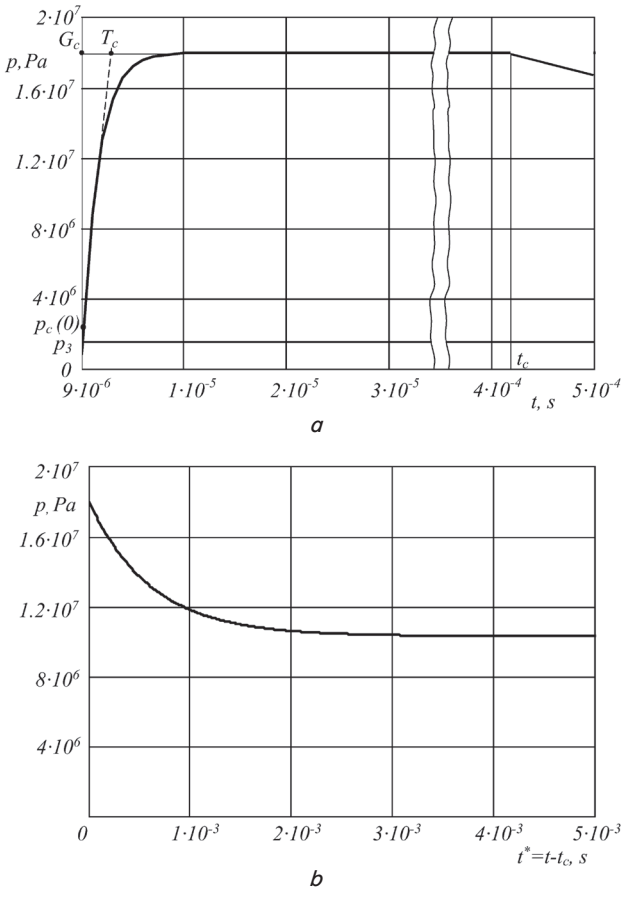

Fig. 6. The change in pressure in the chamber on the segments: *a* – compression ($0\le t\le t_c$); *b* – extensions ($t_c\le t\le T$)

Static characteristics are the dependencies of the steady-state values of the end clearance on the steady-state pressures p_1 and p_3 and the rotor speed ω. To determine them, the current values of the compression and expansion pressures must be replaced by the values averaged over a period T.

The average pressure p_{2c} in the chamber over the compression time t_c is

$$p_{2c}=\frac{1}{t_c}\int_0^{t_c}p_c\mathrm{d}t=G_c-\left(G_c-G_p\right)\frac{T_c}{t_c}\left(1-e^{-\frac{t_c}{T_c}}\right).$$

The curve $p_c(t)$ in the section $0<t<T_c$ practically merges with the ordinate axis, and in the section $T_c<t<t$ the same happens with the horizontal line $G_c\approx p_1$. Thus, as a first approximation, the average pressure in the chamber during the compression period can be taken equal to the compaction pressure of $p_{2c}\approx p_1$.

The expansion process is described by the second equation (5), the solution of which is similar to (8):

$$p'_p=p'_p(0_*)e^{-\frac{t_*}{T_p}}. \tag{10}$$

The expansion begins at the moment the feeder leaves the sector in which the chamber is located, i. e., at the moment t_c when $t_*=0$. The current time in the expansion section is $t_*=t-t_c$. According to the formulae, (6) and (10) are similar to (9):

$$p_p(t_*)=G_p-\left(G_p-G_c\right)e^{-\frac{t_*}{T_p}}.$$

For incompressible fluids, $T_c=T_p=0$, $p_p=G_p=\text{const}$.

The average pressure p_{2p} over the expansion time $T–t_c$ in the chamber is

$$p_{2p}=\frac{1}{T-t_c}\int_0^{T-t_c}p_p\mathrm{d}t_*=$$

$$=G_p-\left(G_p-G_c\right)\frac{T_p}{(T-t_c)}\left[1-\exp\left(-\frac{T-t_c}{T_p}\right)\right].$$

As seen in Fig. 6, the expansion pressure curve $p_p(t)$ asymptotically approaches the horizontal line of $G_p=\alpha_{e3}p_1+\alpha_{e1}p_3$ and differs little from the averaged pressure p_{2p}.

Based on the found expressions of the average pressure on the temporary segments of compression and expansion, we will determine the total average pressure over the entire period between successive injections:

$$p_2=\frac{1}{T}\left[p_{2c}t_c+p_{2p}(T-t_c)\right]. \tag{11}$$

The compression pressure distributed over the entire period is included in (11) with a small factor of t_c/T; the expansion pressure has a factor of $(T–t_c)/T$ close to one. Thus, the main contribution to the averaged pressure is made by the expansion process. Therefore, the existing calculation methods [10, 11] do not take into account the pressure p_{2c}.

After a number of simplifications [16], we will obtain the following formula for calculating the dimensionless value of the averaged pressure in the chambers:

$$\psi_2(u)\approx\alpha_{e3}\psi_1+\alpha_{e1}\psi_3+$$
$$+\alpha_{e1}\cdot\frac{t_n/\Omega-\overline{T}_c+\overline{T}_p/u^3}{T_n}\Omega\Delta\psi, \tag{12}$$

where the first two summands represent the pressure in the gap without feeders, the last two summands with the factors T_p and T_c are the average pressures during expansion and contraction of the liquid in the chamber. The main contribution to the value of $\psi_2(u)$ is made by the addendum $\alpha_{e3}\psi_1$.

Using the linear pressure plots shown in Fig. 3, let us calculate the forces included in the equations of axial equilibrium. The regulatory action is the pressure force F_s on the contact surface, revealing the mechanical gap. The pressure force F_e pressing the ring against the support disk is an external load, and the driving force is the force F_k of the elastic elements.

$$F_s=0.5(p_1+p_2)A_1+p_2A_2+$$
$$+0.5(p_2+p_3)A_3=F_{s0}+Ap_2(u),$$
$$F_{s0}=0.5(A_1p_1+A_3p_3), \tag{13}$$
$$A_1=\pi\left(r_3^2-r_{22}^2\right),\quad A_2=\pi\left(r_{22}^2-r_{21}^2\right),\quad A_3=\pi\left(r_{21}^2-r_1^2\right),$$

$A = 0.5(A_1 + 2A_2 + A_3)$ is the contact area effective with respect to the average pressure in the chamber p_2.

$$F_e = B_1 p_1 + B_3 p_3, \quad F_k = k(\Delta + z), \tag{14}$$

$$B_1 = \pi(r_3^2 - r_4^2), \quad B_3 = \pi(r_4^2 - r_1^2).$$

The pressure force component F_{s0} in the gap and the pressing pressure force F_e do not depend on the size of the mechanical gap.

The equation of axial equilibrium F_s=F_e+F_k, taking into account the fact that the end clearance, is negligible in comparison with the preliminary deformation of elastic elements $z << \Delta$, after substituting forces in (13) and (14), it is reduced to

$$Ap_2 = -0.5(A_1 p_1 + A_3 p_3) + B_1 p_1 + B_3 p_3 + k\Delta, \tag{15}$$

where k is the reduced coefficient of axial stiffness of the elastic elements. We will divide this equality term by Ap_n and move on to dimensionless forces by introducing the following notation:

$$\chi = F_k / Ap_n = k(\Delta + z)/Ap_n \approx k\Delta / Ap_n,$$

$$\phi_e = F_e / Ap_n = \frac{1}{A}(B_1\psi_1 + B_3\psi_3), \tag{16}$$

$$\phi_s = \frac{F_s}{Ap_n} = \phi_{s0} + \psi_2(u), \quad \phi_{s0} = \frac{F_{s0}}{Ap_n} = \frac{1}{2}(A_1\psi_1 + A_3\psi_3),$$

where p_n is the nominal pressure of the liquid being sealed at the inlet. As a result, from (15) we obtain the equilibrium equation of a dimensionless form:

$$\phi_s = \phi_{s0} + \psi_2 = \phi_e + \chi$$

or

$$\psi_2(u) = -\phi_{s0} + \phi_e + \chi. \tag{17}$$

Given (16), we will represent the latter equality in the form of

$$\psi_2(u) = \frac{B_1 - 0.5A_1}{A}\psi_1 + \frac{B_3 - 0.5A_3}{A}\psi_3 + \chi.$$

We will introduce the notation of the dimensionless areas K and σ and reveal the difference of $\phi_e - \phi_{s0}$:

$$K = (B_1 - 0.5A_1)/A, \ \sigma = (B_3 - 0.5A_3)/A = 1 - K,$$

$$\phi_e - \phi_{s0} = K\psi_1 + (1 - K)\psi_3. \tag{18}$$

In this case, equation (17) of the axial equilibrium of the axially movable ring takes the form

$$\psi_2(u) = K\psi_1 + (1 - K)\psi_3 + \chi,$$

where $\psi_2(u)$ is also determined by formula (12). From the joint solution of the equations of the balance of expenses and the equation of axial equilibrium of the axially movable ring, we will express the dependence of the gap on external perturbations ψ1, ψ3, Ω and the driving action χ as

$$K\Delta\psi + \psi_3 + \chi = \alpha_{e3}\psi_1 + \\ + \alpha_{e1}\psi_3 + \alpha_{e1} \cdot \frac{t_n / \Omega - \overline{T}_c + \overline{T}_p / u^3}{T_n} \Omega\Delta\psi.$$

After grouping the terms, we will find the dependence of the end clearance on the compacting pressure drop, on the rotor speed, and on the pre-compression force of the elastic elements, i. e., we will find the desired static characteristic:

$$u = \left\{ \frac{\alpha_{e1} \dfrac{\overline{T}_p}{T_n} \Omega}{\dfrac{\chi}{\Delta\psi} + K - \alpha_{e3} - \alpha_1 \dfrac{t_n - \overline{T}\Omega}{T_n}} \right\}^{1/3}. \tag{19}$$

6. Identification of factors affecting the dynamic characteristics of the seal

Let us consider the axial vibrations of the ring, excited by harmonically changing external influences ψ_1 and ψ_3, relative to the equilibrium position. In centrifugal machines, as a rule, the sealing pressure and the back pressure change with a frequency equal to or a multiple of the rotational speed. The maximum amplitudes have fundamental harmonics with the frequency ω; therefore, the forced oscillations of the ring relative to the position of static equilibrium u_0 will be considered under the influence of dimensionless pressures:

$$u = u_0 + u_a e^{i\omega t}, \ \psi_1 = \psi_{10} + \psi_{1a} e^{i\omega t}, \ \psi_3 = \psi_{30} + \psi_{3a} e^{i\omega t}, \tag{20}$$

where ψ_{10} and ψ_{30} are the constant components of the pressures; ψ_{1a} and ψ_{3a} are the amplitudes of their oscillations, and u_a is the amplitude of the axial oscillations of the ring. The rotation frequency and the setting action change quasistatically, so they only affect the steady-state position of the ring.

In dynamics, the axial vibrations of the ring lead to the appearance of additional flow components. The period of change of these terms is $2\pi/\omega$, and it differs from the periods t_c and $T–t_c$ of the compression and expansion rates caused by pressure pulses supplied to the chamber by the feeders. To facilitate further consideration of these terms in the generalized equation of the balance of expenses, we will consider in more detail the transformation of equations (4):

$$Q_i + Q_1 - Q_3 = \frac{V_0}{E}\left(\frac{dp}{dt}\right)_c, \quad Q_1 - Q_3 = \frac{V_0}{E}\left(\frac{dp}{dt}\right)_p.$$

Having multiplied these equations by $(dt)_c$ and $(dt)_p$, respectively, we turn to the volume balance equations

$$(Q_i + Q_1 - Q_3)(dt)_c = \frac{V_0}{E}(dp),$$

$$(Q_1 - Q_3)(dt)_p = \frac{V_0}{E}(dp)_p,$$

which do not contain time derivatives and can be added summand by summand:

$$Q_i(dt)_c + (Q_1 - Q_3)\left[(dt)_c + (dp)_p\right] = \\ = \frac{V_0}{E}\left[(dp)_c + (dp)_p\right].$$

The sums of the increments of time and pressure cover the entire period T between successive injections; they can thus be denoted as $(\mathrm{d}t)_p+(\mathrm{d}t)=\mathrm{d}t$, $(\mathrm{d}p)_c+(\mathrm{d}p)_p=\mathrm{d}p$:

$$Q_i(\mathrm{d}t)_c+(Q_1-Q_3)\mathrm{d}t=\frac{V_0}{E}\mathrm{d}p.$$

Dividing this equality by dt, we go to the complete equation of the expense balance

$$Q_i\frac{(\mathrm{d}t)_c}{\mathrm{d}t}+Q_1-Q_3=\frac{V_0}{E}\dot{p}.$$

We replace the infinitesimal time increments on the left side of the last equation with the corresponding finite increments $(\mathrm{d}t)_c\approx\Delta t_c=t_c-0=t_c=\beta_c/\omega$, $\mathrm{d}t\approx\Delta T=T-0=T$. As a result, the flow balance equation in the absence of forced axial vibrations takes the form

$$Q_i\frac{t_c}{T}+Q_1-Q_3=\frac{V_0}{E}\dot{p}. \tag{21}$$

The equation obtained with axial vibrations of the axially movable ring excited by harmonic oscillations of external pressures contains two additional terms. They take into account the flow rate of compression-expansion of the fluid in the chambers Q_p and the flow rate of displacement Q_v from the end clearance (sector β_c) with a periodic change in pressure caused by fluctuations in the gap with frequency ω under the influence of external pressures (20) [16]:

$$Q_p=\frac{V_0}{E}p_n\frac{\mathrm{d}\psi}{(\mathrm{d}t)_\omega},\quad Q_v=A_sz_n\frac{\mathrm{d}u}{(\mathrm{d}t)_\omega}, \tag{22}$$

where $A_s=\frac{\beta_c}{2\pi}(A_1+A_2+A_3)$ is the butt surface area of the sector β_c.

The lower index ω indicates that the increment $(\mathrm{d}t)_\omega$ changes in an interval equal to the period $T_0=2\pi/\omega=n_iT$ of axial oscillations. In contrast to the static analysis where the averaged, time-independent pressure $\psi_2=p_2/p_n$ (11) was used, here we are dealing with a time-varying pressure, which we will denote by p without an index but in the dimensionless form $\psi=p/p_n$.

As in the derivation of equation (21), we will replace the differentials with finite increments, i. e., we will use approximate expressions:

$$\frac{\mathrm{d}\psi}{(\mathrm{d}t)_\omega}=\frac{\mathrm{d}\psi}{\mathrm{d}t}\frac{\mathrm{d}t}{(\mathrm{d}t)_\omega}\approx\dot{\psi}\frac{\Delta t}{(\Delta t)_\omega}=\dot{\psi}\frac{T}{T_0}=\frac{1}{n_i}\dot{\psi},$$

$$\frac{\mathrm{d}u}{(\mathrm{d}t)_\omega}=\frac{\mathrm{d}u}{\mathrm{d}t}\frac{\mathrm{d}t}{(\mathrm{d}t)_\omega}\approx\dot{u}\frac{\Delta t}{(\Delta t)_\omega}=\dot{u}\frac{T}{T_0}=\frac{1}{n_i}\dot{u}.$$

Let us substitute them in (22) and add the resulting expressions to the right side

$$Q_i\frac{t_c}{T}+Q_1-Q_3=\frac{V_0}{E}\dot{\psi}\left(1+\frac{1}{n_i}\right)+A_s\frac{z_n}{n_ip_n}\cdot\dot{u}.$$

Having expressed the spending through the pressure drops (3), we arrive at a first-order nonlinear differential equation with respect to the desired dimensionless pressure ψ in the chamber:

$$\left(g_i\frac{t_c}{T}+g_{1n}u^3\right)(\psi_1-\psi)-$$

$$-g_{3n}u^3(\psi-\psi_3)=\frac{V_0}{E}\left(1+\frac{1}{n_i}\right)\dot{\psi}+A_s\frac{z_n}{n_ip_n}\dot{u}. \tag{23}$$

In the future, we will consider the linearized system without taking into account the inertia of the liquid during its unsteady motion. We will linearize the area of the position of static equilibrium, passing to the deviations of the variables in both sides of equation (23). We will also introduce the notations $g_i'=g_it_c/T$; $g_{1n}u_0^3=g_{10}$, $g_{3n}u_0^3=g_{30}$ where g_{10} and g_{30} are the conductivities of the corresponding end throttles for the steady-state gap value of z_0. After a series of transformations, the normalized equation of the balance of expenses in deviations takes the form

$$T_2\dot{\psi}+\psi=-(\tau_2\dot{u}+\kappa_s'u)+k_1\psi_1+k_3\psi_3,$$

where

$$T_2=\frac{V_0}{Eg_{s0}}\left(1+\frac{1}{n_i}\right),\quad \tau_2=\frac{A_sz_n}{n_ip_ng_{s0}},$$

$$k'_s=\frac{3}{g_{s0}u_0}\left[g_{30}(\psi_0-\psi_{30})-g_{10}(\psi_{10}-\psi_0)\right]=$$

$$=\frac{3}{g_{s0}u_0}(k_1g_{30}-k_3g_{10})(\psi_{10}-\psi_{30}), \tag{24}$$

$$k_1=\frac{g_i'+g_{10}}{g_{s0}},\quad k_3=\frac{g_{30}}{g_{s0}},\quad g_{s0}=g_i+g_{10}+g_{30}=g_{sn}u_0^3.$$

If we introduce the time differentiation operator s=d/dt and denote

$$T_2s+1=D_2(s),\quad \tau_2s+k'_s=M_2(s),$$

then we will come to the equation in the operator form with respect to the pressure in the chamber:

$$D_2(s)\psi(t;u)=-M_2(s)u+k_1\psi_1+k_3\psi_3. \tag{25}$$

We will obtain the dynamic equation of the automatic controller by substituting the pressure $\psi(t;u)$, determined by differential equation (25), in the linear expression (16) for the dimensionless force ϕ_s:

$$\psi(t;u)=-\frac{M_2}{D_2}u+\frac{k_1\psi_1+k_3\psi_3}{D_2}.$$

At the same time, the regulatory impact is

$$\phi_s=\psi(t;u)+\phi_{s0}=-\frac{M_2}{D_2}u+\frac{k_1\psi_1+k_3\psi_3}{D_2}+\phi_{s0}$$

and we obtain the controller equation by multiplying both sides of this equality by the differential operator $D_2=T_2s+1$:

$$D_2(s)\phi_s=-M_2(s)u+k_1\psi_1+k_3\psi_3+D_2(s)\phi_{s0}. \tag{26}$$

From equation (26), the dimensionless dynamic stiffness of the system, which is the transfer function of the controller by mistake, is expressed by the formula

$$W_2(s)=\frac{\phi_s}{u}=-\frac{\tau_2 s+k'_s}{T_2 s+1}.$$

The ring is considered as a single-mass system that performs one-dimensional axial vibrations described by the equation

$$m\ddot{z}=F_s-F_e-F_k-c\dot{z},$$

where the term $c\dot{z}$ represents the external (outside the end clearance) linear viscous friction force. The remaining forces are described by formulae (14) and (16) when replacing the averaged pressure in the chamber $\psi_2(u)$ with a pressure of $\psi(t;u)$ that depends on both the gap and time. Using these formulae, we will write

$$m\ddot{z}+c\dot{z}+kz=F_s-F_e-k\Delta=$$
$$=AP+0.5(A_1p_1+A_3p_3)-(B_1p_1+B_3p_3)-k\Delta,$$

and after going over to deviations under the condition that $k\Delta$=const, $\delta(k\Delta)$=0 and after dividing each term by Ap_n, we will get

$$\frac{mz_n}{Ap_n}\ddot{u}+\frac{cz_n}{Ap_n}\dot{u}+\frac{kz_n}{Ap_n}u=\phi_s-\phi_e=$$
$$=\psi+\frac{1}{2A}(A_1\psi_1+A_3\psi_3)-\frac{1}{A}(B_1\psi_1+B_3\psi_3).$$

Let us denote the coefficients of the left side of this equation

$$T_1^2=\frac{mz_n}{Ap_n},\quad 2\xi=\sqrt{\frac{c^2z_n}{mAp_n}},\quad \chi_n=\frac{kz_n}{Ap_n}$$

and use the load factor K (18):

$$\phi_{s0}-\phi_e=-\left[K\psi_1+(1-K)\psi_3\right].$$

In the operator form, we will obtain the final form of the equation of axial oscillations of the ring:

$$D_1(s)u=\phi_s-\phi_e=\psi-K\psi_1-(1-K)\psi_3,$$
$$D_1(s)=T_1^2s^2+2\xi T_1s+\chi_n. \qquad (27)$$

The coefficients have the following physical meaning: T_1 is the period of free vibrations of the axially movable ring; ξ is the damping coefficient of free vibrations due to external linear friction; and χ_n is the dimensionless coefficient of rigidity of the elastic elements.

If the right-hand side of (27) is equal to zero, then the equation

$$D_1(s)u=T_1^2\ddot{u}+2\xi T_1\dot{u}+\chi_n u=0$$

becomes the equation of free axial vibrations of the ring suspended on elastic elements with equivalent rigidity k without taking into account pressure forces. In this case, $\chi_n/T_1^2=k/m=\omega_0^2$; ω_0 is the natural frequency of the axial vibrations of the ring without a regulatory action.

We obtain the equation of dynamics of pulse compaction as an automatic control system by eliminating the force ϕ_s from equations (26) and (27):

$$D_1u=-\frac{M_2}{D_2}u+\frac{k_1\psi_1+k_3\psi_3}{D_2}+\phi_{s0}-\phi\ .$$

Let us multiply both sides of the equality by the operator D_2

$$(D_1D_2+M_2)u=k_1\psi_1+k_3\psi_3+D_2(\phi_{s0}-\phi_e)$$

and group the terms in powers of s, taking into account (18):

$$\left[T_1^2T_2s^3+(T_1^2+2\xi T_1T_2)s^2+\right.$$
$$\left.+(2\xi T_1+\chi_nT_2+\tau_2)s+\chi_n+k'_s\right]u=$$
$$=-\left[KT_2s+K-k_1\right]\psi_1-$$
$$-\left[(1-k_s)T_2s+1-k_s-k_3\right]\psi_3.$$

The expressions in the square brackets represent the operator of the system $D(s)$ and the operators $N_1(s)$, $N_3(s)$ of external influences:

$$D(s)u=-N_1(s)\psi_1-N_3(s)\psi_3, \qquad (28)$$

where

$$D(s)=a_0s^3+a_1s^2+a_2s+a_3,\ N_1(s)=b_0s+b_1,$$
$$N_3(s)=c_0s+c_1, \qquad (29)$$
$$a_0=T_1^2T_2,\ a_1=T_1^2+2\xi T_1T_2,$$
$$a_2=2\xi T_1+\chi_nT_2+\tau_2,\ a_3=k'_s+\chi_n,$$
$$b_0=KT_2,\ \ b_1=K-k_1;\ \ c_0=(1-K)T_2,\ \ c_1=1-K-k_3. \qquad (30)$$

An axially movable ring in the axial direction is affected by a number of perturbations, among which harmonic perturbations with frequencies equal to the rotor speed prevail (20). In the dimensionless form, the pressure deviations are

$$\delta\psi_1\to\psi_1=\psi_{1a}e^{i\omega t},\ \ \delta\psi_1\to\psi_3=\psi_{3a}e^{i\omega t},$$
$$\delta\psi\to\Delta\psi=(\psi_{1a}-\psi_{3a})e^{i\omega t}.$$

Within the framework of the linear compression model under consideration, the superposition principle is valid, i. e., the resulting ring reaction is the sum of harmonic reactions to individual elementary harmonic perturbations. Therefore, the analysis of harmonic axial vibrations of the ring caused by each of the harmonic perturbations is of practical importance. The rotation frequency, as a rule, has the form of a stepwise or linear function of time, and the reaction to it is characterized by time characteristics.

Forced oscillations are characterized by amplitude and phase frequency characteristics, which are the amplitudes and phases of the frequency transfer functions. For equation (28) with two harmonic effects, the frequency transfer functions are written as follows:

$$W_1(i\omega)=\frac{u_{1a}e^{i(\omega t+\gamma_1)}}{\psi_{1a}e^{i\omega t}}=-\frac{N_1(i\omega)}{D(i\omega)}=A_1(\omega)e^{i\gamma_1},$$

$$W_3(i\omega)=\frac{u_{3a}e^{i(\omega t+\gamma_3)}}{\psi_{3a}e^{i\omega t}}=-\frac{N_3(i\omega)}{D(i\omega)}=A_3(\omega)e^{i\gamma_3},$$

where A_1 and A_3 are the amplitude characteristics while γ_1 and γ_3 are the phase frequency characteristics for perturba-

tions ψ_1 and ψ_3, respectively. It can be seen from the above formulae that when the natural operator is equal to zero, the amplitudes increase indefinitely. The corresponding speeds are the natural frequencies of the ring-regulator system.

To express the amplitudes and phases in terms of the coefficients (30), it is necessary to represent the transfer functions as complex numbers in the algebraic form. To do this, in the operators of (29), we will introduce the following changes in d/dt=s=$i\omega$:

$$D(i\omega)=-ia_0\omega^3-a_1\omega^2+ia_2\omega+a_3=U+i\omega V;$$

$$U=a_3-a_1\omega^2,\ \ V=a_2-a_0\omega^2;$$

$$N_1(i\omega)=ib_0\omega+b_1,\ \ N_3(i\omega)=ic_0\omega+c_1.$$

Now the transfer functions take the form

$$W_1(i\omega)=-\frac{b_1+i\omega b_0}{U+i\omega V},\ \ W_3(i\omega)=-\frac{c_1+ic_0\omega}{U+i\omega V}.$$

We will divide the real and imaginary parts of these expressions by multiplying the numerators and denominators by the complex number conjugate to the denominator:

$$W_1(i\omega)=-\frac{(b_1+i\omega b_0)(U-i\omega V)}{U^2+\omega^2V^2}=$$
$$=-(U_1-i\omega V_1)=-A_1(\omega)e^{i\gamma_1},$$

$$W_3(i\omega)=-\frac{(c_1+i\omega c_0)(U-i\omega V)}{U^2+\omega^2V^2}=$$
$$=-(U_3-i\omega V_3)=-A_3(\omega)e^{i\gamma_3}, \qquad (31)$$

$$U_1=-\frac{b_1U+\omega^2b_0V}{U^2+\omega^2V^2},\ \ V_1=\frac{b_1V-b_0U}{U^2+\omega^2V^2},$$

$$U_3=-\frac{c_1U+\omega^2c_0V}{U^2+\omega^2V^2},\ \ V_3=\frac{c_1V-c_0U}{U^2+\omega^2V^2}.$$

The amplitudes and phases of (31) are expressed by the formulae:

$$A_1(\omega)=\frac{u_{1a}}{\psi_{1a}}=\sqrt{U_1^2+\omega^2V_1^2}=\sqrt{\frac{b_1^2+\omega^2b_0^2}{U^2+\omega^2V^2}},$$
$$\gamma_1=-\text{arctg}\omega\frac{b_0U-b_1V}{b_1U+\omega^2b_0V}, \qquad (32)$$

$$A_3(\omega)=\frac{u_{3a}}{\psi_{3a}}=\sqrt{U_3^2+\omega^2V_3^2}=\sqrt{\frac{c_1^2+\omega^2c_0^2}{U^2+\omega^2V^2}},$$
$$\gamma_3=-\text{arctg}\omega\frac{c_0U-c_1V}{c_1U+\omega^2c_0V}.$$

According to the amplitude frequency characteristics, it is possible to estimate the dimensional values of the amplitudes of the forced axial vibrations of the ring at any speed if the magnitude of the amplitudes of the oscillations of the pressure deviations p_{1a}, p_{3a} is set as follows:

$$z_{1a}=A_1(\omega)z_n\,p_{1a}/p_n,\ \ z_{3a}=A_3(\omega)z_n\,p_{3a}/p_n.$$

For the analysis of dynamic stability, the Routh-Hurwitz stability criterion can be used. According to this criterion, the third-order system is stable if all the coefficients (30) of its own operator are positive (the coefficients satisfy this condition). In addition, the inequality $a_1a_2>a_0a_3$, must be satisfied, which, after substituting the values of the coefficients, is reduced to

$$2\xi\left[T_1^2+T_2\left(2\xi T_1+\chi_nT_2\right)\right]>T_1\left(k'_sT_2-\tau_2-2\xi\frac{T_2}{T_1}\tau_2\right).$$

If external damping $(c=\xi=0)$, is not taken into account, then the stability condition reduces to the inequality

$$\tau_2>T_2k'_s, \qquad (33)$$

from which there is a stability margin with some tolerance.

After substituting the values of (24) in (33), it is possible to determine the chamber volume admissible in stability:

$$V_0<\frac{A_sEz_0g_{s0}}{3(1+n_i)(k_1g_{30}-k_3g_{10})(p_{10}-p_{30})}. \qquad (34)$$

Since k'_s~$\Delta\psi$ (24), the dynamic stability condition must be satisfied for the maximum possible working differential pressure of the liquid being sealed, i. e., for the value of the stiffness coefficient corresponding to $\Delta\psi_{\max}$.

7. An example of engineering calculations for the pulse mechanical seal

We will consider the engineering calculation procedure using an example of a pulse mechanical seal similar to one stage of the main circulation pump seal for nuclear power plants with a VVER-1000 reactor.

The initial data are r_0=0.115 m, p_1=(4÷16) MPa, p_3=0, p_n=p_{1n}=10 MPa, and ω=ω_n=150 s^{-1}.

The sealed medium is water, μ=10^{-3} Pa·s, E=2.2·103 MPa.

For the design purposes, the dimensions of the contact surface are the following: r_1=r_0+0.005=0.12 m, r_3=0.14 m, r_2=0.5(r_1+r_3)=0.13 m, r_{21}=0.128 m, r_{22}=0.132 m, l_1=l_3=0.08 m, as well as the size and number of chambers and feeders: n_i=4, n_c=32, $V_0\approx3\cdot10^{-7}$ m^3, d_i=0.4·10^{-3} m, l_i=8·10^{-3} m, $\beta_s=2\pi/n_c=0.196\approx1.6\beta_c$ and $\beta_c=b_c/r_2=0.123$ rad.

We will calculate the area of the end sections:

– $A_1=\pi\left(r_3^2-r_{22}^2\right)=6.84\cdot10^{-3}$ m^2;
– $A_2=\pi\left(r_{22}^2-r_{21}^2\right)=3.27\cdot10^{-3}$ m^2;
– $A_3=\pi\left(r_{21}^2-r_1^2\right)=6.23\cdot10^{-3}$ m^2;
– $A_c=64\cdot10^{-6}$ m^2;
– A=0.5(A_1+2A_2+A_3)=9.8·10^{-3} m^2.

The determined parameters are the conductivity of the end throttles and their dimensionless values, the time constants of filling and emptying of the chambers, and weight coefficients. The calculation results are given in Tables 1–3 for 5 values of the nominal clearance. This will allow us to evaluate the effect of z_n on the static characteristics.

Let us calculate the coefficient of hydrostatic stiffness (Table 4).

As a result, k_s<0, i. e., the equilibrium stability condition, is satisfied for 5 values of z_n.

We will calculate the load factor K_n, which provides the nominal clearance in the nominal mode of $\Delta\psi\approx\Omega\approx1$, as well as the load area B_1 and the inner radius r_4 corresponding to this value (Table 5).

Table 1

Butt throttle conductivity

z_n, μm	g_i	g_{1n}	g_{3n}	g_{en}
3	$7.854 \cdot 10^{-11}$	$4.843 \cdot 10^{-15}$	$4.428 \cdot 10^{-15}$	$2.313 \cdot 10^{-15}$
4		$1.148 \cdot 10^{-14}$	$1.05 \cdot 10^{-14}$	$5.483 \cdot 10^{-15}$
6		$3.875 \cdot 10^{-14}$	$3.542 \cdot 10^{-14}$	$1.851 \cdot 10^{-14}$
8		$9.184 \cdot 10^{-14}$	$8.397 \cdot 10^{-14}$	$4.386 \cdot 10^{-14}$
10		$1.794 \cdot 10^{-13}$	$1.64 \cdot 10^{-13}$	$8.567 \cdot 10^{-14}$

Table 2

Dimensionless conductivities

z_n, μm	α_{1i}	α_{3i}	α_{e1}	α_{e3}
3	$6.166 \cdot 10^{-5}$	$5.638 \cdot 10^{-5}$	0.48	0.52
4	$1.462 \cdot 10^{-4}$	$1.336 \cdot 10^{-4}$		
6	$4.933 \cdot 10^{-4}$	$4.51 \cdot 10^{-4}$		
8	$1.169 \cdot 10^{-3}$	$1.069 \cdot 10^{-3}$		
10	$2.284 \cdot 10^{-3}$	$2.088 \cdot 10^{-3}$		

Table 3

Time constants of filling and emptying chambers as well as weighting factors

z_n, μm	G_c	G_p	T_c	T_p	T_n	t_c
3	10^7	$5.224 \cdot 10^6$	$1.736 \cdot 10^{-6}$	0.015	0.01	$8.2 \cdot 10^{-4}$
4	10^7		$1.736 \cdot 10^{-6}$	$6.205 \cdot 10^{-3}$		
6	$9.995 \cdot 10^6$		$1.735 \cdot 10^{-6}$	$1.839 \cdot 10^{-3}$		
8	$9.989 \cdot 10^6$		$1.732 \cdot 10^{-6}$	$7.756 \cdot 10^{-4}$		
10	$9.979 \cdot 10^6$		$1729 \cdot 10^{-6}$	$3.971 \cdot 10^{-4}$		

Table 4

Coefficients of hydrostatic stiffness

z_n, μm	3	4	6	8	10
k_s	–0.5	–0.21	–0.06	–0.03	–0.014

Table 5

Values of compaction parameters

z_n, μm	K_n	B_1, m^2	r_4, m
3	1.231	0.015	0.121
4	0.843	0.012	0.126
6	0.644	$9.726 \cdot 10^{-3}$	0.128
8	0.595	$9.251 \cdot 10^{-3}$	0.129
10	0.578	$9.082 \cdot 10^{-3}$	0.129

The numerical evaluation of the effect of the pre-compression force of elastic elements will be performed for its three values: χ=0.004; 0.01; and 0.03.

We will construct static (Fig. 7) and consumption (Fig. 8) characteristics.

The dynamic calculation consists in constructing the amplitude and phase frequency characteristics for external influences ψ_1 and ψ_3.

Of practical interest are, first of all, the amplitude frequency characteristics. The results of their calculation for various values of the nominal gap are shown in Fig. 9.

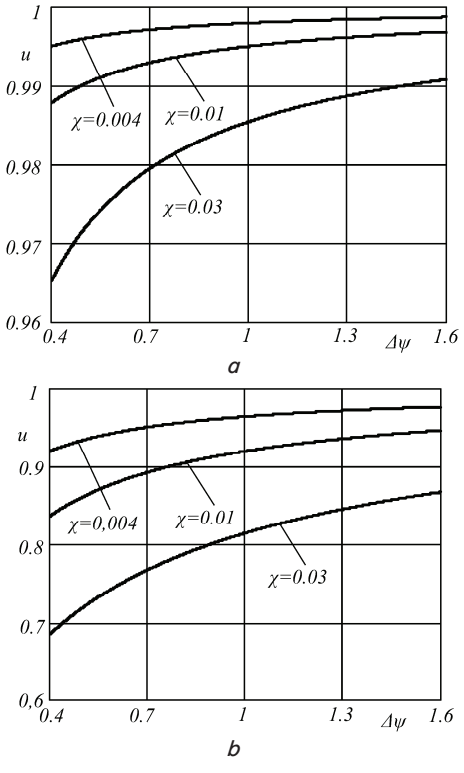

Fig. 7. Static characteristics for various nominal gaps z_n: *a* – z_n=3 μm; *b* – z_n=8 μm

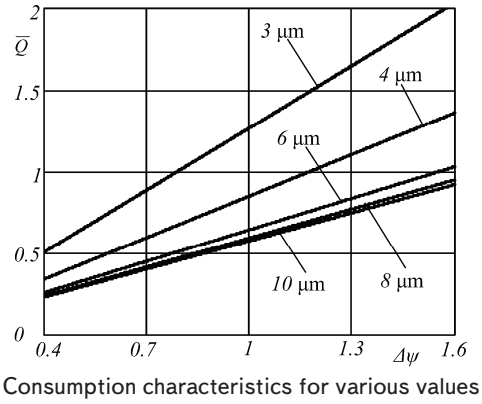

Fig. 8. Consumption characteristics for various values of the nominal clearance z_n

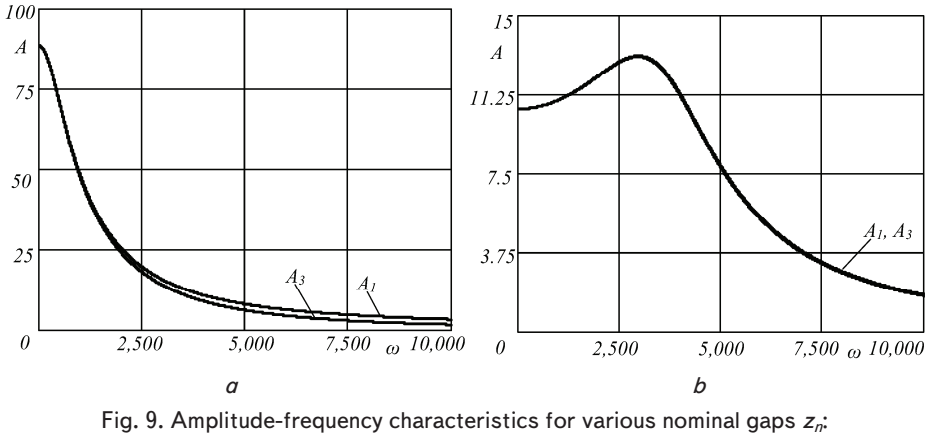

Fig. 9. Amplitude-frequency characteristics for various nominal gaps z_n: *a* – z_n=3 μm; *b* – z_n=8 μm

8. An MCP shaft sealing system based on pulse seals

Rotor sealing is one of the most complex and critical components of the MCP that determines the reliability of the entire unit. This is explained by the difficult operating conditions of the seals in combination with high requirements for tightness at nominal, transient and emergency operations of the pump.

The seal assembly (Fig. 10) consists of seals such as inner 1, main 2, closing 3, and end 4. The inner seal 1, which is a set of three floating rings, separates the chamber *A*, where cold water is supplied, from the sealing cavity *B* of the pump. On the floating rings, the end contact belts are made on both sides. In the event of an emergency drop in the pressure of the locking water, the rings operate on a pressure difference that is changed in the direction, and the entire assembly provides the required tightness for 40 s. The pressure drop across the inner seal is maintained within 0.1–0.5 MPa; the inner and outer diameters of the rings are 200 mm and 210 mm.

The main seal 2 is two series-connected stages of the pulse end seal. The same stage 3 serves as a closing seal, which should briefly perform the functions of the main in case of failure of the latter. The end seal 4 is a simple ring throttle.

The sealing system includes a line for supplying shut-off water to the chamber *A* by high-pressure feed pumps through a hydrocyclone 6. Water throttled on the main seals 2 is cooled in heat exchangers 5. In case of failure of the shut-off water supply system, the alarm system is activated: the valve 7 opens through the cooler 8 and the hydrocyclone 6 enters the chamber *B*, ensuring the normal long-term operation of the seal. If necessary, part of the controlled leakage through the throttle device 9 can be returned to the supply line of the locking water.

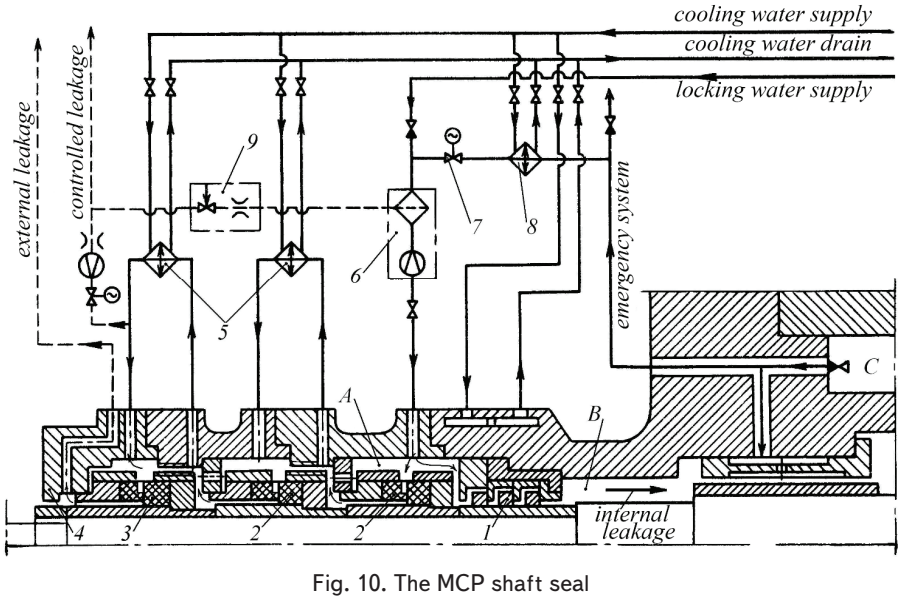

Fig. 10. The MCP shaft seal

The accumulated experience of industrial operation shows that pulsed end seals meet the stringent requirements for reliability, durability and tightness, which are imposed on the seals of the rotors of NPP pumping equipment [1].

9. Discussion of the results of studying the characteristics of the pulse mechanical seal

The physical model of a pulse mechanical seal as a system for automatically controlling the mechanical clearance and leaks has been built. This made it possible to apply the methods of the theory of automatic control to derive analytical dependencies describing their operation.

The analysis of the static characteristics revealed the influence of the design parameters of pulse compaction on the size of the end clearance. It can be seen from formula (19) that an increase in the steady-state value of the end clearance leads to an increase in the parameters of $\Delta\psi$, Ω, $\overline{T}_p$ and n_i as well as a decrease in K, χ, $\overline{T}_c$ and z_n.

The characteristics obtained during the engineering calculations (Figs. 7, 8) show that in the given pressure range of the liquid being sealed, the end clearance differs little from the base value, which ensures optimal working conditions. An increase in the dimensionless compressive force of the elastic elements χ leads to a decrease in the gap.

The obtained expressions of the amplitude and phase frequency characteristics (32) make it possible to identify dangerous regions of rotational frequencies and select the sealing parameters so that the amplitudes of the forced axial vibrations of the ring could not go beyond the permissible limits.

Factors affecting the dynamic stability of pulse compaction were identified. The resulting expression (33) shows that stabilization is facilitated by an increase in the displacement time constant τ_2, a decrease in the compression time constant T_2 and the hydrostatic coefficient of rigidity k'_s.

From formula (34) for determining the chamber volume that is acceptable for stability it follows that the stability region expands, first of all, due to a decrease in the chamber volume and a decrease in the hydrostatic stiffness coefficient. The obtained expressions allow, due to the selection of the geometric parameters of compaction, to provide a stability boundary with a certain margin.

The restrictions adopted during the development of the methodology for calculating pulse seals were that the pressure change in the end clearance section with a constant gap is linear in its radius, and the inertia forces of the liquid in the mechanical gaps are small. The authors believe that the assumptions made do not distort the qualitative picture of the ongoing processes, and taking into account calculations with a certain margin, they are quite acceptable for practical use. This is confirmed by the successful experience in the industrial operation of pulse seals developed and designed using the developed calculation methodology. One of the engineering calculations applied in practice is given in the work as an example.

It should be noted that the operation of pulse seals is accompanied by complex non-stationary, high-frequency hydrodynamic processes in the friction pair. This opens up a wide field for study, since a rather large number of questions remain regarding the features of the operation of seals of this type under various conditions that require further research.

10. Conclusion

1. A physical model of a pulse mechanical seal was constructed as a system for automatically controlling the mechanical clearance and leaks. The dependencies of the size of the end clearance and flow rate were obtained for the liquid being sealed against the differential sealing pressure, the rotor speed, and the pre-compression forces of the elastic elements. The results of the study made it possible to evaluate the effect of the design parameters of the seal on the change in its performance. The study showed that the pulse seal design provides non-contact operation, automatically maintaining a gap in the range of 3–10 μm, while external leakage remains in the range of 5–10 l/hr.

2. The expressions were obtained for the amplitude and phase frequency characteristics, which made it possible to identify dangerous regions of rotational frequencies and select the sealing parameters so that the amplitudes of the forced axial vibrations of the ring could not go beyond the limits of dynamic stability. The stability region expands by reducing the volume of the chambers and by a decrease in the coefficient of hydrostatic stiffness. The tests showed that in pulse seals, with an increase in the rotation frequency, the end clearance increases slightly; as a result, the increase in the friction power is limited. Seals have virtually no speed limits, so their use is especially effective for high-speed machines.

References

1. Martsinkovskiy, V. A., Shevchenko, S. S.; Shevchenko, S. S. (Ed.) (2018). Nasosy atomnyh elektrostantsiy: raschet, konstruirovanie, ekspluatatsiya. Sumy: ChF «Izdatel'stvo «Universitetskaya kniga», 472.
2. Martsinkovski, V., Gaft, J., Zagorulko, A., Gromyko, B. (2003). Design and calculation of mechanical seals with self-adjusting clearance. Papers presented at 17th International Conference on Fluid Sealing. York, UK, 505–520.
3. Martsynkovskyy, V., Gaft, Y., Gromyko, B., Chernov, O. (2000). Development and application of double pulse gas-liquid seals. Proc. of 16th International Conference on Fluid Sealing. Brugge, 255–269.
4. Shahin, I. (2016). Gas Seal Performance and Start up Condition Enhancing with Different Seal Groove Geometries. Journal of Aeronautics & Aerospace Engineering, 05 (04). doi: https://doi.org/10.4172/2168-9792.1000177
5. Qiu, Y., Khonsari, M. M. (2012). Thermohydrodynamic Analysis of Spiral Groove Mechanical Face Seal for Liquid Applications. Journal of Tribology, 134 (2). doi: https://doi.org/10.1115/1.4006063
6. Ma, C., Bai, S., Peng, X. (2016). Thermo-hydrodynamic characteristics of spiral groove gas face seals operating at low pressure. Tribology International, 95, 44–54. doi: https://doi.org/10.1016/j.triboint.2015.11.001
7. Ding, X., Lu, J. (2016). Theoretical analysis and experiment on gas film temperature in a spiral groove dry gas seal under high speed and pressure. International Journal of Heat and Mass Transfer, 96, 438–450. doi: https://doi.org/10.1016/j.ijheatmasstransfer.2016.01.045
8. Neuberger, S., Bock, E., Haas, W., Lang, K. (2014). Gas-lubricated mechanical face seals reduce CO_2 emissions. Sealing Technology, 2014 (9), 8–12. doi: https://doi.org/10.1016/s1350-4789(14)70343-5
9. Wang, Y., Yang, H., Wang, J., Liu, Y., Wang, H., Feng, X. (2009). Theoretical Analyses and Field Applications of Gas-Film Lubricated Mechanical Face Seals with Herringbone Spiral Grooves. Tribology Transactions, 52 (6), 800–806. doi: https://doi.org/10.1080/10402000903115445
10. Błasiak, S., Kundera, C. (2012). A Numerical Analysis of the Grooved Surface Effects on the Thermal Behavior of a Non-Contacting Face Seal. Procedia Engineering, 39, 315–326. doi: https://doi.org/10.1016/j.proeng.2012.07.037
11. Zhu, W.-B., Wang, H.-S., Zhou, S.-R. (2014). Research on sealing performance of hydrostatic pressure mechanical seal. Journal of Marine Science and Technology, 22 (6), 673–679. doi: http://doi.org/10.6119/JMST-014-0321-1
12. Blasiak, S., Zahorulko, A. V. (2016). A parametric and dynamic analysis of non-contacting gas face seals with modified surfaces. Tribology International, 94, 126–137. doi: https://doi.org/10.1016/j.triboint.2015.08.014
13. Martsynkovskyy, V., Zahorulko, A., Gudkov, S., Mischenko, S. (2012). Analysis of Buffer Impulse Seal. Procedia Engineering, 39, 43–50. doi: https://doi.org/10.1016/j.proeng.2012.07.006
14. Marcinkowski, W. A., Kundera, Cz. (2008). Seft-controlled face seal. Pomiary-Automatyka-Kontrola, 5, 270–272.
15. Blasiak, S. (2019). Numerical modelling and comparison analysis of pressure distribution in the gas film for non-contacting face seals. EPJ Web of Conferences, 213, 02005. doi: https://doi.org/10.1051/epjconf/201921302005
16. Gaft, J., Zahorulko, A., Martsynkovskyy, V., Kundera, Cz. (2012). Theoretical and experimental investigations of buffer face impulse seals. 11th EDF/Pprime Workshop: "Behaviour of Dynamic Seals in Unexpected Operating Conditions". doi: http://doi.org/10.13140/RG.2.1.4062.9204